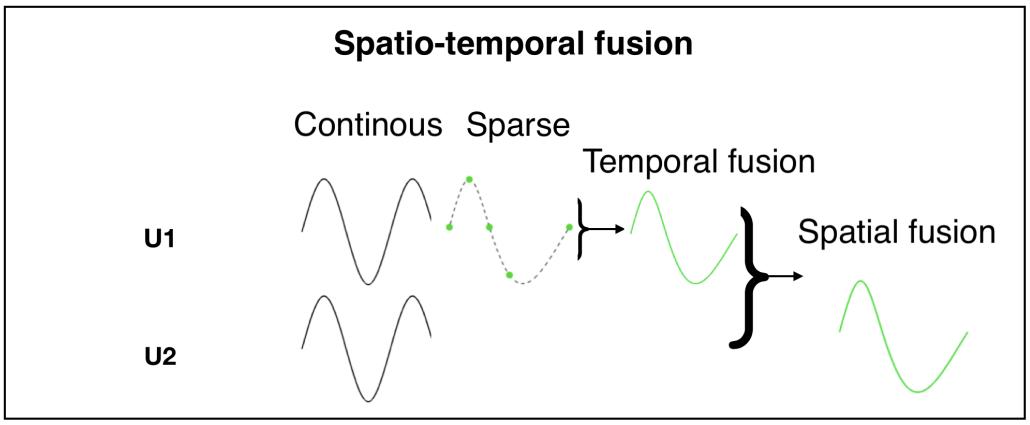

Graphical Abstract

A hybrid solution for offshore wind resource assessment from limited onshore measurements.

Basem Elshafei, Alfredo Pena, Dong Xu, Jie Ren, Jake Badger, Felipe M. Pimenta, Donald Giddings, Xuerui Mao

Highlights

A hybrid solution for offshore wind resource assessment from limited onshore measurements.

Basem Elshafei, Alfredo Pena, Dong Xu, Jie Ren, Jake Badger, Felipe M. Pimenta, Donald Giddings, Xuerui Mao

- A novel algorithm is proposed to merge limited high-fidelity measured data and continuous low-fidelity simulation results.
- The proposed method using a gappy onshore measurement results in accurate offshore wind resource assessment within a 7% margin error, significantly outperformed the industry standard method.

A hybrid solution for offshore wind resource assessment from limited onshore measurements.

Basem Elshafei[a], Alfredo Pena[b], Dong Xu[c], Jie Ren[a], Jake Badger[b], Felipe M. Pimenta[d], Donald Giddings[a], Xuerui Mao[a,]

[a]*Faculty of Engineering, University of Nottingham, NG7 2RD, Nottingham, UK*
[b]*DTU Wind Energy, Technical University of Denmark, Roskilde, Denmark*
[c]*Xinjiang Goldwind Science and Technology Co., Ltd, PR China*
[d]*Centro de Ciências Físicas e Matemáticas, Campus Trindade, Universidade Federal de Santa Catarina Florianópolis, SC 88010-970, Brazil*

Abstract

In wind resource assessments, which are critical to the pre-construction of wind farms, measurements by LIDARs or masts are a source of high-fidelity data, but are expensive and scarce in space and time, particularly for offshore sites. On the other hand, numerical simulations, using for example the Weather Research and Forecasting (WRF) model, generate temporally and spatially continuous data with relatively low-fidelity. A hybrid approach is proposed here to combine the merit of measurements and simulations for the assessment of offshore wind. Firstly a temporal data fusion using deep Multi Fidelity Gaussian Process Regression (MF-GPR) is performed to combine the intermittent measurement and the continuous simulation data at an onshore location. Then a spatial data fusion using a neural network with Non-linear Autoregression (NAR) and Non-linear Autoregression with external input (NARX) are conducted to project the wind from onshore to offshore. The numerical and measured wind speeds along the west coast of Denmark were used to evaluate the method. We show that the proposed data fusion technique using a gappy onshore measurement results in accurate offshore wind resource assessment within a 7% margin error.

Keywords:
Artificial neural network, Gaussian process regression, Spatiotemporal data fusion, Wind resource assessment

Email address: xuerui.mao@nottingham.ac.uk (Xuerui Mao)

1. Introduction

In the past decades, there has been worldwide demand for renewable energy, leading to a dramatic expansion in all its sectors, with a significant fraction generated by wind. There are over 230 GW of installed wind capacity in Europe as of 2020, consisting of 190 GW onshore and 40 GW offshore. Additionally, Europe intends to further the rise in demand for wind energy and its capacity by 35% [1]. Before the construction of a wind farm, it is critical to evaluate the wind speed condition of the location. Since the power is the cube function of wind speed, minor speed changes can cause large deviations in the output power. Moreover, the wind varies both geographically and temporally over a wide range of scales. Therefore, an accurate assessment of the wind resource for a proposed site is highly essential and is considered of paramount significance for a wind project to be successful [2],[3]. The assessment also helps to the selection of wind turbines and their layouts [4].

Physical wind measuring devices include Light Detection and Ranging (LIDARs), meteorological mast towers, Satellite Synthetic Aperture Radars (SARs), and so forth. These equipment yield accurate results but are expensive and the data is commonly sparse in space and time. For example, the SARs measured wind is at 10 m above the sea surface with low temporal resolution and only applies to offshore assessments; LIDARs measure the Line-Of-Sight (LOS) velocity by computing the Doppler shift of the signal of an infrared laser beam based on the movement of aerosols and the output is usually intermittent at a fixed location; buoy systems are expensive and require periodic maintenance, redundant systems for power, measurements, and communication for the measurement at a given location. On the contrary, numerical simulations result in wind predictions that cover large geographical areas and long time horizons continuously, but with relatively low fidelity. The numerical models include Weather Research and Forecasting (WRF), Global Forecast System (GFS), and European Centre for Medium-Range Weather Forecasts (ECMRWF), etc. [5].

Such a clear complement of physical measurements and numerical information suggests data fusion or a hybrid technique to combine the merit of both. It would be very desirable to extend the information from coastal online vertical LIDARs for the reconstruction of offshore time series as they

are easier to maintain [6]. This technique can be used to numerically extend the information from coastal measurements to the offshore time series with low cost and high accuracy. Such techniques have been widely used in the prediction of future developments based on various inputs [7]. For example, Hu and Wang [8] used Empirical Wavelet Transforms (EWT), Partial Auto-Correlation Function (PACF), and GPR for wind speed assessments. EWT was employed to extract the meaningful data from the wind speed series through a customized wavelet filter bank, and PACF provided the input parameters for the GPR to simulate dynamic features and internal uncertainties. An alternative combination, i.e. Auto-Regressive (AR) and GPR, was followed by Zhang and Wei [6]. AR was employed to capture the structure of the wind speed series, and GPR to extract the local structures. As a supplement, Automatic Relevance Determination (ARD) considered the importance of using different inputs; thus, various types of covariance functions were combined to comprehend the characteristics of the data. This hybrid method outperformed other methods including Support Vector Machine (SVM), Artificial Neural Network (ANN), and the persistence approach. Meanwhile, an improved near-surface wind speed prediction experiment, which considered the atmospheric stability using GPR combined with Numerical Weather Prediction (NWP), for a time horizon of 72 hours, showed that the consideration of atmospheric stability was able to reduce the estimated errors, thus improving power predictions [2].

Most recently, the Multi-Fidelity Gaussian Process Regression (MF-GPR) has been demonstrated to significantly outperform the regular single fidelity model. The strategy of MF-GPR was to go beyond the regular AR kriging scheme and introduce more than one dataset at different fidelity levels. The first is a high-fidelity, scarce dataset which can be the physically measured one; the second is a low-fidelity, continuous dataset which can be generated from numerical simulations. The literature in this area further discussed various developments; for example, the Deep MF-GPR with additional datasets, e.g. first and second derivatives, phase-shifted oscillations, and different periodicity datasets leading to drastically improved approximations [11].

Further, wind resource assessments are commonly requested over a long-time-interval (e.g. a few months or years) and to cover large areas, therefore requiring spatial-temporal fusion of numerically and physically measured wind [12]. Apart from the temporal prediction reviewed above, ANNs are trained and tested on datasets from two different locations. Cadenas and Rivera, considered the problem of non-linearity in the time-series us-

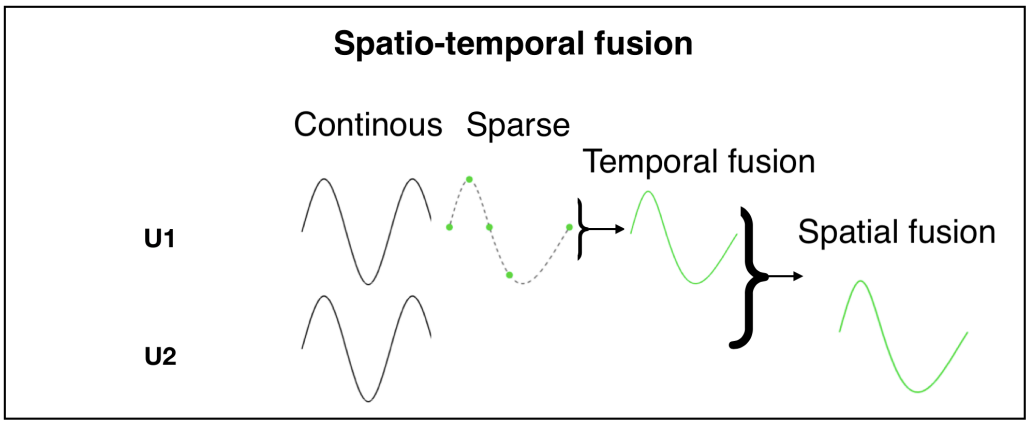

Figure 1: Flow chart for spatiotemporal fusion. U1 and U2 represent the wind speed at two positions. In the test case in this work they correspond to onshore and offshore wind, respectively, and the continuous and sparse data is from measurements and simulations, respectively.

ing Nonlinear Auto-Regressive with Exogenous inputs (NARX) [10]. The method was compared with both the persistence approach and Nonlinear Auto-Regressive (NAR). The results demonstrated that the NARX model was the most precise of the three and justified the extra input, suggesting that it could be suitable for spatial data fusion.

Spatiotemporal models which combine the aforementioned temporal and spatial fusion, have been widely used in the geostatistics field, where temperature and wind speed were the main variables of concern. In these models, the temporal extrapolation is performed to predict the values out of the measured interval at a fixed spatial point [13], followed by spatial extrapolation to project the estimation to a different point [14]. This sequential extrapolation in time and space was developed in the present study for wind resource assessment. Temporal data fusion of low and high-fidelity data from simulations and measurements at a given location was performed using deep MF-GPR, and spatial data fusion using a customised nonlinear autoregressive ANN with exogenous inputs was conducted thereafter. As illustrated in Figure 1, the low fidelity results (e.g from numerical simulations) are assumed to be available across a continuous domain $X \times T$, where X and T are the spatial and temporal domains, respectively. On the other hand, high-fidelity results (e.g from the LIDAR measurements) are available in a reduced domain $X_{re} \times T_{re}$ where X_{re} is a subset of X and can be discon-

tinuous and T_{re} is a subset of T and can be discontinuous. Thereafter, the objective was to combine the low and high-fidelity results to reach a data fusion on the full domain $X \times T$. In practice, this is an assessment of offshore wind from numerical simulations tuned by limited onshore measurements.

2. Methodology

2.1. Temporal data fusion

In this section, we introduce the algorithms for temporal data fusion by combining the low-fidelity continuous time series and the high-fidelity intermittent one. In Section 2.1.1. the prototype of the Gaussian process regression is briefly introduced and then multi-fidelity GPR is presented in Section 2.1.2. The use of different co-variance functions such as constant, linear, squared exponential, Matern and rational quadratic, defines the method of prediction for the Gaussian process.

2.1.1. Gaussian Process Regression (GPR)

GPR is a non-parametric, stochastic process that follows the Bayesian approach for regression, working well on small data sets and having the ability to provide uncertainty measurements on predictions. Predictions are derived using a probability distribution over all possible values of a time-series using prior functions w of training points f at observed points t, and targeted values f^* at unobserved points t^* are calculated from a predictive distribution, $p(f^*|t^*, f, t)$, by considering all possible predictions using their calculated posterior distribution:

$$p\left(f^*|t^*, f, t\right) \;=\; \int p\left(f^*|t^*, w\right) p\left(w|f, t\right) dw. \tag{1}$$

To trace the integration process of equation (1), all terms of the equation are assumed Gaussian. The prior function defines the Gaussian distribution:

$$f(t) \sim GP(m, k(t, t')), \tag{2}$$

where m is the mean function, which represents the trend of the function, and the covariance function (kernel), $k(t, t')$, represents the dependence of the structure, defined by the hyperparameters [15].

2.1.2. Multi-fidelity Gaussian Process Regression

In this section, we discuss advanced temporal data fusion using data with multiple fidelities to enhance the accuracy of prediction. The data sets are obtained using different techniques mathematically, the multi-fidelity technique considers the high-fidelity model as a function of two variables (t, s) and then uses the low-fidelity data as the s variable:

$$f_h(t) = g(t, f_1(t)), \tag{3}$$

where in the present work $f_h(t)$ and $f_l(t)$ are the high-fidelity LIDAR measurements and low fidelity WRF simulations, respectively. Such non-linear auto-regressive Gaussian process (NARGP) has been observed to produce highly accurate prediction when $f_h(t)$ is non-linearly dependent on $f_l(t)$, and GPR is then performed in a two-dimensional space.

To implement this, we adopt the co-kriging model, which uses multivariate functions with respect to different levels of fidelities to reflect different accuracies. The additional data set is later introduced to the Gaussian distribution and we add the terms of the first data set (t, s) and the second data set (t', s') while the mean function is zero, through:

$$f(t) \sim GP(m, k((t, s), (t', s'))), \tag{4}$$

Merging of two or more sets that are approximately linearly dependent by scaling and shifting parameters was approached by Kennedy and O'Hagan [16]. However, due to the presence of nonlinear dependencies generally between the datasets, the quality of results degraded as a major issue for linear data fusion algorithms. To overcome and resolve the nonlinear dependencies, space-dependent scaling factor $\rho(x)$ [17] or alternatively, deep multi-fidelity GP [18] was introduced. Yet the improvement brings further optimizations of additional hyperparameters. Here the NARGP algorithm, an implicit automatic relevance determination (ARD) weight, is employed in the extended space, parametrized by t and s, which counts as a different scaling of the existing hyperparameters for each dimension in the kernel [19].

Additionally, the formulation can be extended through functions of the low-fidelity data set. The high-fidelity data can be further considered as a function t, $f_l(t)$ and the derivatives of $f_l(t)$, exploiting that $f_l(t)$, has a similar trend with $f_h(t)$:

$$f_h(t) = g(t, f_l(t), f_l^1(t), ...f_l^i(t)), \tag{5}$$

where $f_l^i(t)$ is the i-th derivative of the low fidelity data.

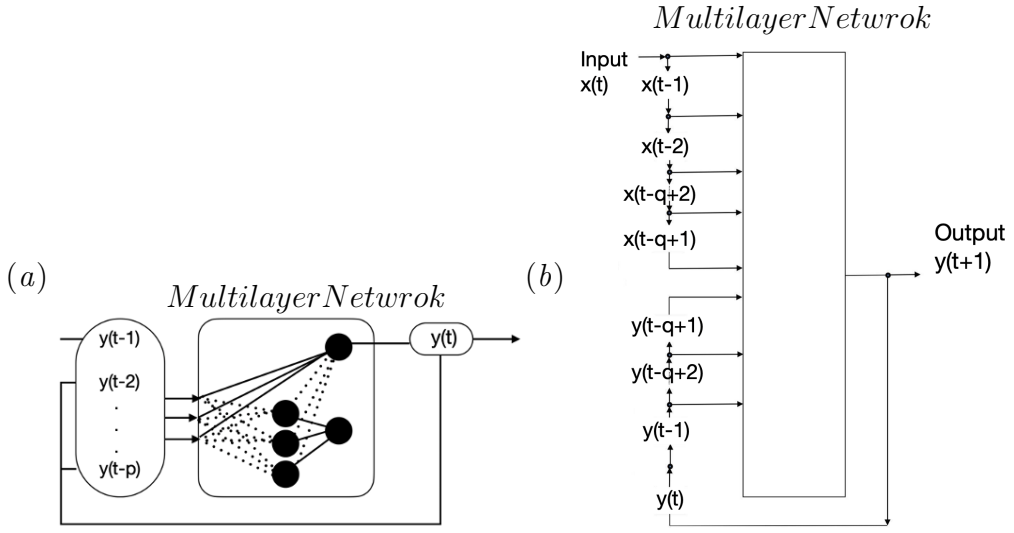

Figure 2: (a) Architecture of the NAR (nonlinear autoregressive) model with a multi layer perception. (b) Framework for NARX model with an exogenous variable x as the input. q past values of x and y are considered for the prediction of y(t+1).

2.2. Spatial extrapolation

As aforementioned the target is to predict offshore wind indirectly from onshore measured wind. Therefore apart from the temporal fusion algorithms presented above, a spatial extrapolation is required. Here a time series neural network is adopted to link the wind speed at the two points using a single variable nonlinear network NAR along with NARX to have a fair performance comparison. In practice, low-fidelity WRF data will be used to train the network and onshore hybrid solution (obtained by temporal fusion) is served as input to estimate the offshore wind.

2.2.1. Nonlinear Autoregression (NAR)

The NAR model is most suitable for time-series predictions where the main source of training data is only past values of the time series itself, and this process is called feedback delays. The network is trained in an open loop, which uses the real target values as a response. Following, the network becomes a closed-loop, and the predicted values are used as new response inputs to the network. The framework of this model as seen in Figure 2(a), a multi-layer network where the left hand side is the past delayed input values

$y(t-1), y(t-2)$, and $y(t-p)$ is used to obtain the independent variable $y(t)$. Optimisation of the network aims to reduce the number of synapses (weights) and neurons, and subsequently reducing the complexity of the network, and maintaining the generalisation capabilities.

2.2.2. Nonlinear Autoregression with External Input (NARX)

NARX is a dynamically guided type of recurrent ANN, which contain one or more feedback loops. The loops can be either local or regional, and the use of regional loops enables a significant reduction of memory requirements [9]. Moreover, different models of NARX networks are comprised of the same structure and thus have a reasonable cost from a computational point of view. The previous argument allows a NARX network to gain degrees of freedom when it includes a time-frame forecast. As input data in subsequent periods compared to a feed-forward network, it allows the synthesis of information from exogenous variables and less inclusion of their remains, reducing the number of parameters to be calculated.

Learning in NARX networks is more efficient than in other neural networks (the descending gradient is stronger in NARX). The model predicts a series $y(t)$ given specific past values of $y(t)$ and additional input series $x(t)$ as shown in Figure 2(b). Dynamically, this is expressed by:

$$y(n+1) = F(y(n), y(n-q+1), u(n), u(n-q+1)), \tag{6}$$

where q is the total number of delayed memory neurons, the output $y(t+1)$ is the predicted value representing the one step ahead variable and F is a nonlinear function.

As it was proven essential to have at least two-thirds of the data for the training part, the training, validation, and test divisions, were partitioned to meet 60 percent training, 20 percent validation, and 20 percent testing, respectively. We constructed 10 hidden neurons with 2 delays, and adopted the Bayesian regularisation as the training algorithm trades off more computational costs for better accuracy [9].

3. Case description

To test the methods, we consider a case associated with the RUNE project, which was a near-shore experiment conducted at the west coast of Denmark (see Figure 3 (a)). The surrounding area is nearly flat coastal farmland and moving northwards from position 1 to 3, the sand embankment

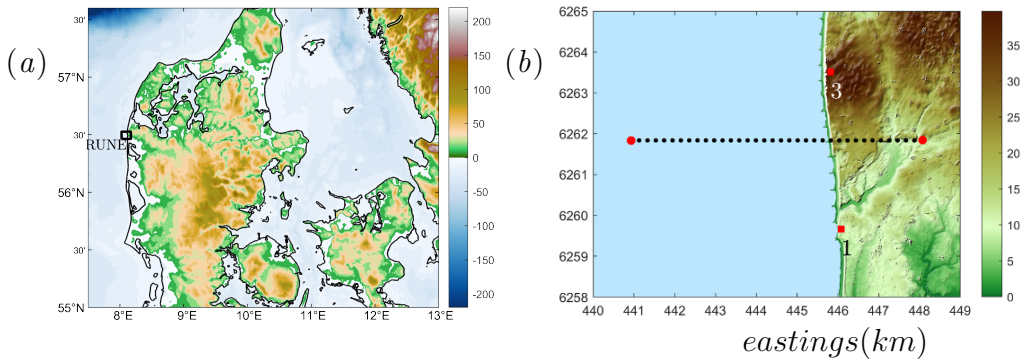

Figure 3: (a) The location of the RUNE experiment (black rectangle) in Denmark. (b) RUNE experimental area. Positions of the LIDARs are shown in red markers and the dual-Doppler scans in black markers.

separating the North Sea and the grasslands transforms into cliffs covered by grass. In this work, we use dual-Doppler scans performed nearly perpendicular to the coast from about 5 km offshore to 2 km onshore. These scans were performed by synchronising measurements from two scanning LIDARs, which are modified versions of WLS200S Leosphere units, one located at position 1 and the other at position 3. Here, we use the dual-Doppler scans performed at 50 m above mean sea level (amsl) during the period 2015-12-08 to 2016-02-17. Due to filtering of high noise/low signal strength and system availability, only 114 10-min are available at all the dual-Doppler positions shown as black markers in Figure 3 (b). Further details with regards to the experimental campaign and the instrumentation can be found in [20].

Here we use a numerical experiment, which was part of a number of numerical simulations performed using the WRF model v3.6 to supplement the measurements of RUNE [22]. This particular experiment was setup with 4 nested domains, the outermost covering northwestern Europe and a 2-km horizontal resolution innermost domain covering the west coast of Denmark. Spectral nudging to the ERA5 reanalysis is used in the upper model levels of the outermost domain. The simulation had 8 vertical levels within the first 100 m and instantaneous output was produced every 10 min. The experiment also used the Mellor-Yamada Janjic planetery boundary layer scheme, a sea surface temperature product from the Danish Meteorological Institute [21], and the CORINE land cover description. An illustration of the low fidelity WRF simulation data set of the most onshore point can be seen in Figure

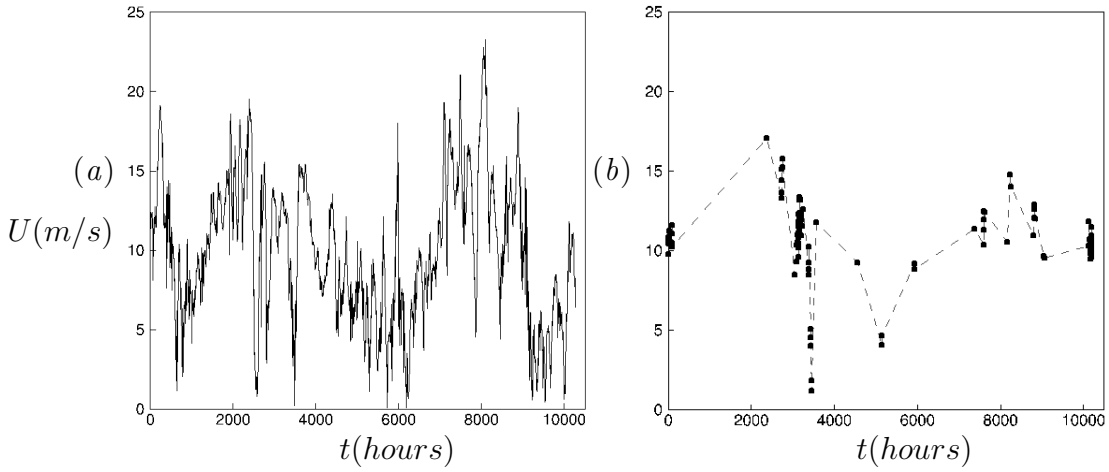

Figure 4: (a) Low-fidelity data from numerical simulation (WRF) at the most onshore point, (see Figure 3).(b) High-fidelity data from scanning LiDAR at the most onshore point, (see Figure 3).

$4(a)$, while Figure $4(b)$ shows the high fidelity LIDAR measurements for the same point.

4. Data Preprocessing

EWT is used to smooth the given wind speed time-series, using an appropriate wavelet filter bank to GPR. In previous wind speed time series filtering works, signals were pre-processed by either the wavelet transform (WT) or empirical mode decomposition (EMD), both capable of removing noise from the time series [8]. However, the EMD technique lacks any mathematical theory and is sensitive to both sampling and noise, whilst WT is not capable of self-adaption as the model requires parameters specified beforehand. EWT shows promising advantages and eliminates the drawbacks of the others. The process can be divided into five steps [8]:

1. Extending the signal.
2. Fourier transforms.
3. Extracting boundaries.
4. Building a filter bank.
5. Extracting the sub band.

As various studies demonstrated, we use a three-level decomposition as it is capable of achieving good forecasting results for a non-stationary time series, such as wind power and wind speed series.

The original wind speed signal had considerable high-frequency fluctuations. The three-level decomposition attained by the EWT algorithm describes the wind speed series in a meaningful way. Three uncorrelated filter modes were extracted from the wind speed series and a residual was also obtained from the extraction. The reconstructed wind speed series shows a significant decrease in fluctuations and will be served as input to the third GPR model.

5. Results

5.1. Temporal data fusion

Table 1: Configurations and accuracy of the GPR models.

Model	Basis and Kernel functions	RMSE [m/s]
WRF	-	1.24
Hybrid (1)	Zero, Matern 5/2	1.15
Hybrid (2)	Constant, Rational quadratic	1.01
Hybrid (3)	Zero, Matern 3/2	0.86

The different data sets at the furthest onshore point of the dual-Doppler line were merged by applying MF-GPR. The performance of the three models was optimized, through the hyperparameters, by applying 30 iterations of basis and kernel function combinations, including: Zero, Linear, Constant and Matern 5/2 and 3/2; Rational Quadratic, squared Exponential, etc. Firstly, we explored the original model, represented as Hybrid (1), where the input information was low and high-fidelity data sets. Then, we showed that introducing additional information sets, which are functions of the low fidelity data set (first and second derivatives) can enhance the accuracy of predictions, hence Hybrid (2). The third model, Hybrid (3), involved preprocessing of the training set using the EWT reconstruction algorithm, the regenerated first and second derivative sets of the low fidelity data, and finally the North and East decomposed wind speed vector components. A higher drop in RMSE was noted from the Original WRF data.

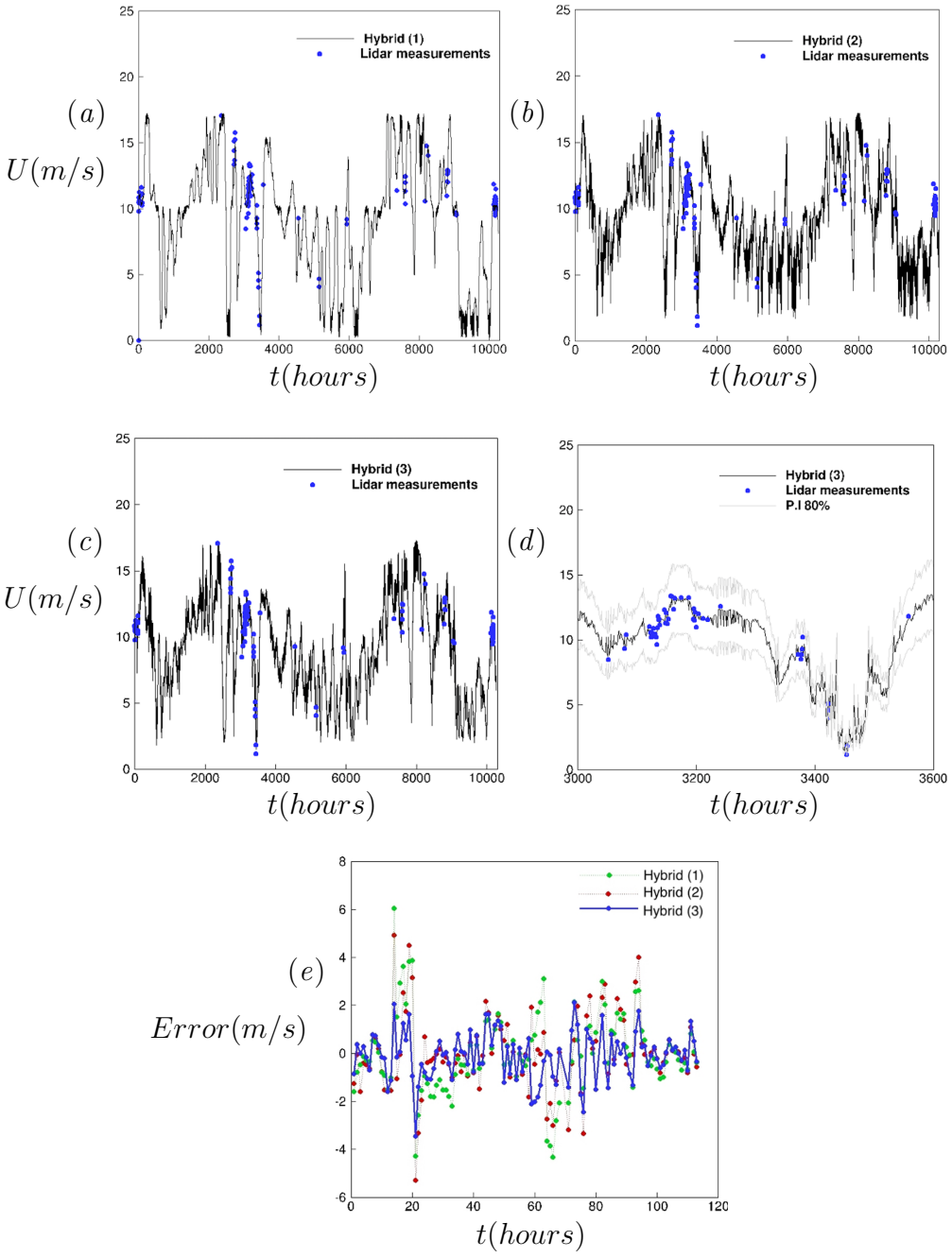

Figure 5: (a), (b) and (c) represent temporal data fusion results for Hybrids (1), (2) and (3), respectively. (d) Cut-off panel for Hybrid (3) from 500 to 600 hours of the experiment and (e) Error in all three hybrid models against 114 LIDAR measurements.

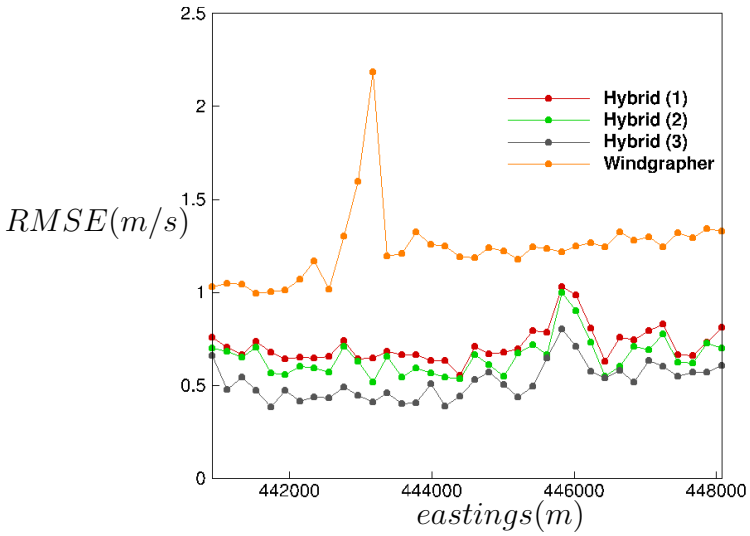

Figure 6: RMSE curve across Windgrapher and all three hybrid models for all 36 dual-Doppler points.

Table 1 shows the RMSE for the best performing GPRs for the three hybrid models and WRF data using the LIDAR data as the ground truth, for each model as well as their respective basis and kernel function configuration. It can be seen that the third model outperformed the other two in terms of RMSE superbly.

Figure 5 panels (a), (b) and (c) show the time series of the results from the three hybrid models, respectively. Hybrid (1) showed a 9% decrease in RMSE from WRF data, in Hybrid (2) the RMSE was reduced by about 18%, and finally Hybrid (3) showed the largest drop compared to other hybrid models, about 31%. Besides, panel (d) reflected a cut off to the interval between the hours 500-600 since the start of the experiment, with an 80% confidence interval, showing a better visualization of the performance. Finally, panel (e) presents the deviation error between the provided high-fidelity time series of 114 points with their predicted counterparts by the hybrid techniques. It can be seen that for some points, Hybrids (1) and (2) outperform each other with deviations ranging from 6 to 2 m/s. On the other hand, the performance of Hybrid (3) outperformed the other two at almost all measured points with the deviation capped at 2 m/s and mean deviation 0.6 m/s. These results substantiate that increasing the number of additional sets and pre-processing the data enhanced the accuracy of the Gaussian process [17].

Furthermore, on a separate iteration, we compare the three hybrid methods against that in Windgrapher, the leading industrial software for importing, visualizing, and analyzing wind resource data. Windgrapher follows the Measure-Correlate-Predict (MCP) algorithms including Linear Least Squares (LLS); the method is on correlating target and reference speed data, based on the linear least squares' procedure.

In Figure 6, we compare the results from the three Hybrid techniques to Windgrapher by calculating the RMSE of results across all 36 dual-Doppler positions from the furthest offshore point to the most onshore one. On average, Hybrids (1), (2), and (3) were able to perform 12%, 14%, and 60%, respectively, more accurately than the industrial software.

5.2. Spatial data fusion

Table 2: Configurations of the NARX and NAR Networks with the Best Performance.

Model	Delays and Neurons	Time steps	MSE ($\times 10^{-}2$)
NAR	3, 15	Training (6176)	1.352
		Validation (2058)	
		Test (2058)	1.559
NARX	4, 12	Training (6176)	1.241
		Validation (2058)	
		Test (2058)	1.188

The spatial data fusion aimed to project the onshore measurements to offshore locations in light of numerical simulations, to reduce the cost of direct offshore measurements. The first and last offshore and onshore points in the 36 dual-Doppler line were considered as an example. An ANN was trained using the low-fidelity WRF data at both points, and it configured the winds' relation at both points. The network was later tested on the high-fidelity LIDAR data of the onshore point and generated high fidelity wind speed results for the offshore point [15].

For the NARX model, eleven simulations were performed varying the number of past values (delays) for the entry variables from 1 to 10, and the number of hidden neurons from 3 to 21. The MSE of the test data set was used to assess the performance of the network, the configuration with the best performance was employed. The same number of simulations were

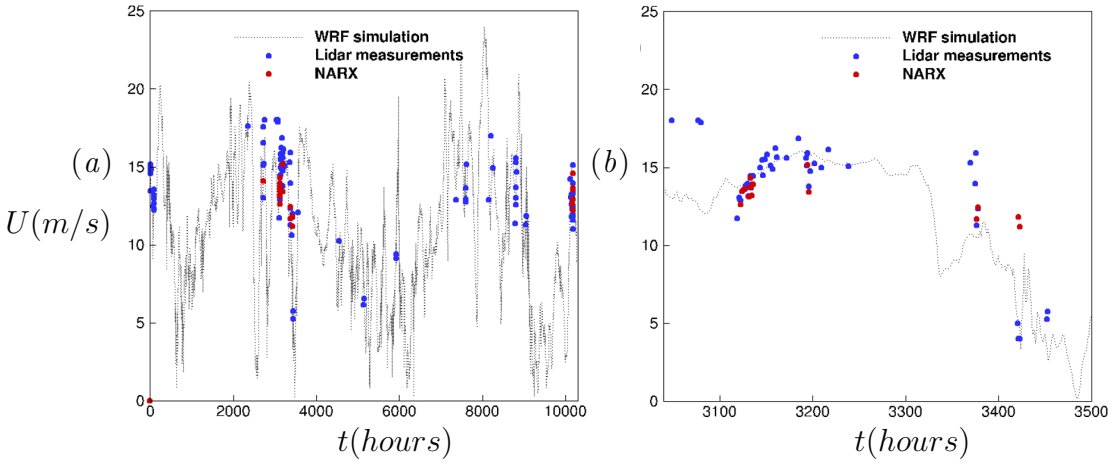

Figure 7: (a) Spatial data fusion results for the offshore point. (b) Close-up of spatially predicted data and high and low-fidelity data for validation.

carried for the NAR model; similarly, the past values varied from 1 to 10 and the hidden neurons from 3 to 15 and the configuration with the lowest MSE was selected.

Figure 7(a) shows the results from testing the NARX network using the LIDAR measurements along with low-fidelity WRF data and high-fidelity LIDAR measurements of the most offshore point. Predicted values from the network were more accurate than the low-fidelity data, where the RMSE was reduced from 1.23 m/s to 1.17 m/s. For a zoomed-up visualization of results, the data-rich high-fidelity section at hours 433-600 is shown in Figure 7(b).

5.3. Spatio-temporal extrapolation

In this section, we combined temporal and spatial data fusion. The aim was to use the intermittent measurement at the most onshore point to estimate the wind at the most offshore point by exploiting the numerical data.

Temporal data fusion was performed following the same technique as Hybrid (3) of MF-GPR from Section 2.1.2., we used the reconstructed set from the EWT algorithm for pre-processing and five predictors for the GPR algorithm: low-fidelity WRF data, first and second derivatives, North and East vector components of the wind speed set of the onshore point. Again, 30-iterations were used to optimize the hyperparameters, varying the basis and kernel functions to achieve a configuration with an RMSE of 0.96 m/s.

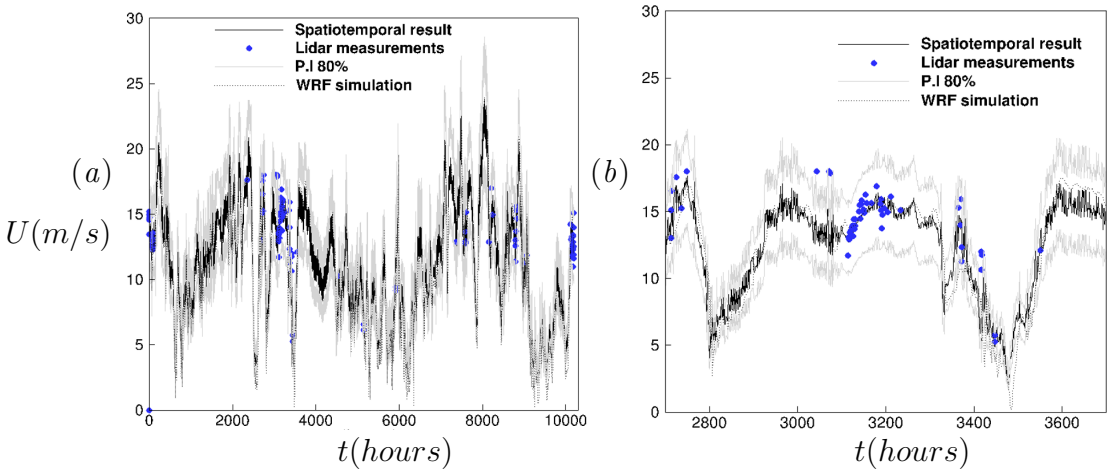

Figure 8: (a) Response for Spatio-temporal data fusion. (b) Close-up of the final spatiotemporal results ranging from hours: 3000-3600.

Following, a NARX neural network was trained using the low-fidelity WRF data of both the most onshore and offshore points with 3 delays and 12 hidden neurons. The network was later tested on the time series generated from the temporal section using MF-GPR and the resulted RMSE of this process was 1.183 m/s.

Figure $8(a)$ shows the final curve of the spatial-temporal data fusion process, high-fidelity LIDAR data (hidden in the assessment), and 80% prediction intervals. In addition, Figure $8(b)$ is a cut-off to show the region with the richest LIDAR data, the results were satisfactory, as it achieved an accurate result with an RMSE 1.29 m/s impersonating the high-fidelity data of the most offshore point without discontinuity or using expensive LIDARs offshore. These results outperformed the WRF simulation at the offshore location where the RMSE was 1.46 m/s, an estimated 12% improvement.

6. Conclusions

In this work, we performed data fusion of numerical model results from WRF simulations (low fidelity), continuous in space and time with LIDAR measurements sparse in time and space (high fidelity) to obtain a spatial-temporal extrapolation, suitable for the assessment of offshore wind. The RUNE experiment performed dual-Doppler scans nearly perpendicular to

the coast, which generated 114 10-minute measurements over three months. Simultaneously, for low-fidelity WRF simulations, numerical simulations performed using the WRF model v3.6 generated an instantaneous output every 10 minutes for the same period of 3 months.

For time-domain data fusion, the effect of pre-processing the data by applying a filter and increasing the number of predictors to include the decomposed vector components of wind speed showed a major drop in the RMSE. This was because we increased the amount of information given to the regression model and reduced fluctuations in the time series, which allowed for improved GPR, hence improved assessment. We were able to represent the high-fidelity data at unobserved regions and periods by exploiting the low-fidelity data and its functions. The addition of extra information datasets and pre-processing showed an improvement in the prediction performance in terms of RMSE, with a 30% average drop compared to other models that ignored them. For the spatial fusion part of the experiment, similarly, adding extra information datasets to the NARX neural network showed improved results compared to the single input model NAR. The data from the network had a lower MSE for assessing offshore data, which could avoid sending expensive equipment offshore. Furthermore, adjusting the neurons and the number of past training values contributed to varying accuracy.

Following data fusion in both space and time, and as aforementioned, the main aim of this study was to combine both methods and perform data fusion in both domains: spatial-temporal extrapolation. The models were re-run at the observed optimized levels in each method: Data from the most onshore point underwent Hybrid (3) MF-GPR for time-domain data fusion, and the output continuous time series was used along with data from the offshore point for space domain data fusion. Finally, the spatial-temporal data fusion resulted in accurate offshore wind resource assessment within a 7% margin error for wind speed. Additionally, the results from the 36 dual-Doppler points, across the offshore-onshore segment, were compared to Windgrapher industrial software, which analyses wind resource data. The comparison of models favoured results from data fusion models of this paper, as all three Hybrid models outperformed the industrial software by at least 40%. Specifically, Hybrid (3) proposed in this work by almost 60%.

Different adaptations, tests, and improvements have been left for the future. Future work concerns further development to the multi-fidelity data fusion algorithm, by introducing additional sources of data generated by different equipment or software. An example of this is the use of a second WRF

simulation with different resolutions and features. Nevertheless, concerning the results for one point-based prediction, we can also expect to perform 3-dimensional area predictions with respect to time, by performing data fusion of multiple LIDAR measurements at different locations with full grid WRF simulation results.

7. Acknowledgement

This project has received funding from the European Union Horizon 2020 research and innovation programme under the Marie Skłodowska-Curie grant agreement No 777717 and the future and emerging technologies programme with agreement No. 828799.

References

[1] M. Negnevitsky, P. Johnson, and S. Santoso. Short term wind power forecasting using hybrid intelligent systems. 2007.

[2] Victoria Hoolohan, Alison S. Tomlin, and Timothy Cockerill. Improved near surface wind speed predictions using gaussian process regression combined with numerical weather predictions and observed meteorological data. *Renewable Energy*, 126, 2018.

[3] K. S.R. Murthy and O. P. Rahi. A comprehensive review of wind resource assessment, 2017.

[4] A. M. Sempreviva, R. J. Barthelmie, and S. C. Pryor. Review of methodologies for offshore wind resource assessment in european seas, 2008.

[5] Shikha Singh, T. S. Bhatti, and D. P. Kothari. A review of wind-resource-assessment technology. *Journal of Energy Engineering*, 132, 2006.

[6] Chi Zhang, Haikun Wei, Xin Zhao, Tianhong Liu, and Kanjian Zhang. A gaussian process regression based hybrid approach for short-term wind speed prediction. *Energy Conversion and Management*, 126, 2016.

[7] Saurabh S. Soman, Hamidreza Zareipour, Om Malik, and Paras Mandal. A review of wind power and wind speed forecasting methods with different time horizons. 2010.

[8] Jianming Hu and Jianzhou Wang. Short-term wind speed prediction using empirical wavelet transform and gaussian process regression. *Energy*, 93, 2015.

[9] Yunhua Li, Lina Ling, and Jiantao Chen. Combined grey prediction fuzzy control law with application to road tunnel ventilation system. *Journal of Applied Research and Technology*, 13, 2015.

[10] Erasmo Cadenas, Wilfrido Rivera, Rafael Campos-Amezcua, and Roberto Cadenas. Wind speed forecasting using the narx model, case: La mata, oaxaca, méxico. *Neural Computing and Applications*, 27, 2016.

[11] Kirthevasan Kandasamy, Gautam Dasarathy, Junier Oliva, Jeff Schneider, and Barnabás Póczos. Multi-fidelity gaussian process bandit optimisation. *Journal of Artificial Intelligence Research*, 66, 2019.

[12] Julija Tastu, Pierre Pinson, Ewelina Kotwa, Henrik Madsen, and Henrik Aa Nielsen. Spatio-temporal analysis and modeling of short-term wind power forecast errors. *Wind Energy*, 14, 2011.

[13] Jingwen Liu, Yanlei Gu, and Shunsuke Kamijo. Customer pose estimation using orientational spatio-temporal network from surveillance camera. *Multimedia Systems*, 24, 2018.

[14] Ramon Dalmau, Marc Pérez-Batlle, and Xavier Prats. Estimation and prediction of weather variables from surveillance data using spatio-temporal kriging. volume 2017-September, 2017.

[15] Miltiadis Alamaniotis and Georgios Karagiannis. Integration of gaussian processes and particle swarm optimization for very-short term wind speed forecasting in smart power. *International Journal of Monitoring and Surveillance Technologies Research*, 5, 2018.

[16] M. C. Kennedy and A. O'Hagan. Predicting the output from a complex computer code when fast approximations are available. *Biometrika*, 87, 2000.

[17] Dave Higdon, Dominique Picard, L. Parussini, D. Venturi, P. Perdikaris, and G. E. Karniadakis. Multi-fidelity gaussian process regression for computer experiments thèse dirigée par josselin garnier thèse rapportée par. *Journal of Computational Physics*, 336, 2017.

[18] P. Perdikaris, M. Raissi, A. Damianou, N. D. Lawrence, and G. E. Karniadakis. Nonlinear information fusion algorithms for data-efficient multi-fidelity modelling. *Proceedings of the Royal Society A: Mathematical, Physical and Engineering Sciences*, 473, 2017.

[19] Carl Edward Rasmussen and Christopher K. I. Williams. *Gaussian Processes for Machine Learning*. 2018.

[20] Rogier Floors, Alfredo Peña, Guillaume Lea, Nikola Vasiljević, Elliot Simon, and Michael Courtney. The rune experiment-a database of remote-sensing observations of near-shore winds. *Remote Sensing*, 8, 2016.

[21] Jacob L. Høyer and Ioanna Karagali. Sea surface temperature climate data record for the north sea and baltic sea. *Journal of Climate*, 29, 2016.

[22] R. Floors, A. N. Hahmann, and A. Peña. Evaluating mesoscale simulations of the coastal flow using lidar measurements. *Journal of Geophysical Research: Atmospheres*, 123, 2018.